Predicting Spatial Field Values Under Undulating Terrain With 2W-PE Based on Machine Learning

Anqi Li, Chengyou Yin, *Member, IEEE*, and Qianqian Zhang

***Abstract*—A two-way parabolic equation (2W-PE) method based on machine learning is proposed to predict the spatial field strength of radio waves propagating over undulating terrain. The method first performs longitudinal domain decomposition on a step distance, and uses different algorithms to solve the 2W-PE in each subdomain. Then, a simple obstacle model (SOM) containing three stepping units of different heights is introduced. A variety of undulating terrains can be approximated using the overlay combinations and lateral extensions of multiple SOMs, and combined with machine learning method, the boundary condition coefficients in different environments can be determined. The simulation results show that the proposed 2W-PE method is in good agreement with the method of moments (MoM), which verifies its accuracy and superiority.**

***Index Terms*—Domain decomposition (DD) method, impedance boundary condition (IBC), machine learning, two-way parabolic equation (2W-PE).**

I. Introduction

WHEN radio waves propagate in the real world, the undulation of the ground will change the paths of radio waves, thereby increasing the transmission process complexity, and affecting the radio signal transmission. Thus, it is important to study radio wave propagation in complex environments.

The traditional two-way parabolic equation (2W-PE) was proposed by Ozgun [1]. Furthermore, the stepped terrain model (STM) can be used to approximate irregular terrain. Combined with impedance boundary conditions (IBC), it is possible to solve radio wave propagation problems on irregular terrain [2]. Due to fast calculation speed and good numerical stability, 2W-PE has gradually become a common method in field calculations [3]–[5]. However, it does not consider propagation inside obstacles, which will cause large errors in the calculation when the inclination angle of the terrain is large.

Regarding the above-mentioned problems, Li [6] introduced the principle of domain decomposition (DD), in which an area with an obstacle is divided into subdomains above and inside the obstacle. Discrete mixed Fourier transformation (DMFT) and finite difference (FD) method are used to solve the 2W-PE, combined with the Leontovich impedance boundary and global IBC (GIBC). However, the instability of GIBC may cause the field value to diverge. In [7], we introduced the surface IBC into 2W-PE for the first time to achieve calculation stability, but its applicable situation is too simple.

In the field of radio wave propagation calculations, machine learning methods can overcome the shortcomings of the original empirical and deterministic models, and they have superior performance in path loss calculations [8], [9], but they are only applicable in fixed propagation environments [9]. Hence, in this letter, we consider using artificial neural networks (ANNs) to adaptively adjust the BC parameters and combining them with 2W-PE to construct a semiempirical and semideterministic prediction model, which can not only improve the accuracy of 2W-PE but also extend its applicability to any propagation scene.

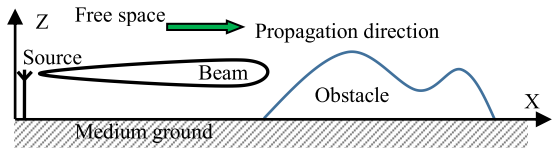

Fig. 1. Schematic diagram of radio wave propagation problem.

II. Framework of the Problem

The radio wave propagation scene is shown in Fig. 1. This study adopts the time specification exp ($j\omega$t), where ω is the angular frequency. Assuming that k is the wavenumber in a homogeneous environment of the medium, n represents the modified refractive index of the atmosphere and obstacles. Field Ψ satisfies the following two-dimensional (2-D) wave equation:

$$\frac{\partial^2 \Psi}{\partial x^2} + \frac{\partial^2 \Psi}{\partial z^2} + k^2 n^2 \Psi = 0 \tag{1}$$

where, in the cases of horizontal polarization and vertical polarization, Ψ can be respectively defined as

$$\Psi(x,z) = E_y(x,z) = E_y \mathbf{e}_y, \Psi(x,z) = H_y(x,z) = H_y \mathbf{e}_y. \tag{2}$$

Here, the positive x-axis is the propagation direction. For forward and backward waves, we introduce a demodulation factor to demodulate the field strength

$$\begin{cases} \psi(x,z) = u_f(x,z) \cdot e^{-\mathrm{j}kx} + u_b(x,z) \cdot e^{\mathrm{j}kx} \\ u_f(x,z) = e^{\mathrm{j}kx} \psi_f(x,z) \quad u_b(x,z) = e^{-\mathrm{j}kx} \psi_b(x,z) \end{cases}. \tag{3}$$

Manuscript received September 2, 2021; revised September 28, 2021 and October 8, 2021; accepted October 12, 2021. Date of publication October 29, 2021; date of current version February 3, 2022. *(Corresponding author: Chengyou Yin.)*

The authors are with the National Key Laboratory of Pulsed Power Laser Technology College of Electronic Engineering, National University of Defense Technology, Hefei 230037, China (e-mail: 935727910@qq.com; cyouyin@sina.com; zeqqian@sina.com).

Digital Object Identifier 10.1109/LAWP.2021.3123836

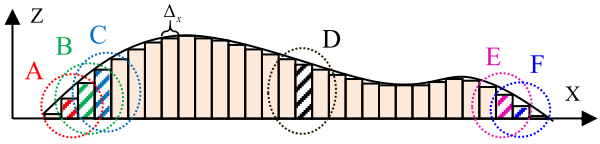

Fig. 2. Schematic diagram of subdivision.

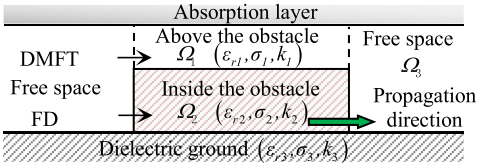

Fig. 3. Schematic diagram of DD algorithm.

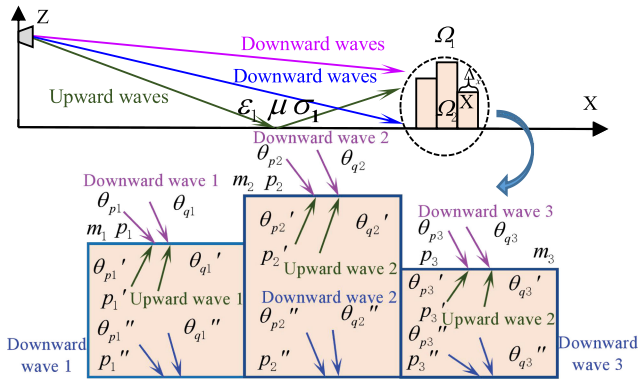

Fig. 4. Schematic diagram of wave propagation and parameters in SOM.

The parabolic equations of forward and backward propagation by the demodulation are as follows [10]:

$$\begin{cases} \frac{\partial u_f}{\partial x} = jk\left(1-Q\right)u_f \\ \frac{\partial u_b}{\partial x} = jk\left(Q-1\right)u_b \end{cases}, \quad Q=\sqrt{\frac{1}{k^2}\frac{\partial^2}{\partial z^2}+n^2\left(x,z\right)}. \tag{4}$$

In the calculation, the initial field of 2W-PE is directly solved by the actual current distribution on the antenna, and the incident source environment is unified with that of method of moments (MoM) [11].

III. Calculation Process of Spatial Field Strength

We first use STM to approximate the undulating terrain in Fig. 1 with a combination of flat-topped obstacles as shown in Fig. 2. The unit width of STM is set to Δ_x according to the obstacle fluctuation speed and the beam width of the wave, which is also the solution step of 2W-PE.

A. Longitudinal DD Calculation

For the case of rectangular flat-topped obstacles, we introduced the 2W-PE algorithm based on the DD method [7] to calculate the spatial field strength inside and outside the obstacle. As shown in Fig. 3, the DD algorithm decomposes the calculating area into subdomains above and inside the obstacle, which are respectively denoted as Ω_1 and Ω_2. The flat terrain area before and after the obstacle can be denoted as Ω_3. We can set IBCs to represent interactions between the subdomains. Thus, the IBC on the lower boundary of Ω_1 can be written as

$$\frac{\partial u}{\partial z}+\mathrm{K}\cdot\ u=0 \tag{5}$$

and the IBCs on the upper and lower boundaries of Ω_2 are

$$\frac{\partial u}{\partial z}+H\cdot\ u=0, \frac{\partial u}{\partial z}+\Lambda\cdot\ u=0 \tag{6}$$

where K, H, Λ are coefficients determined by the wave existing on the boundaries. Since there are no obstacles in Ω_3, we adopt the Leontovich BC on the lower boundary. Then, we can use DMFT [12] to calculate the field value combined with IBCs. As Ω_2 is a limited area, we can discretize the field value points inside the area and use FD combined with the upper and lower IBCs of Ω_2 in (6) to solve the 2W-PE.

B. Lateral Terrain Extension Processing

According to Section III-A, DMFT and FD are used to solve the 2W-PE in the longitudinal direction at each step. Then, we consider extending the calculation of a single flat-top obstacle to the case of undulating terrain. As shown in Fig. 2, although the terrain is represented as the superposition of various small rectangular obstacles, each with a width of Δ_x, located at different distances, the incident field on the boundaries of each single flat-top obstacle is bound to be affected by others. If the impact of all flat-top obstacles is considered, the problem is too complicated, so we only consider the impact of the front and rear flat-top obstacles on the incident field at the boundary of the rectangular cell. Therefore, we divide the original undulating terrain into several simple obstacle models (SOMs), each with a width of $3\Delta_x$, according to the starting position. These SOMs are superimposed on each other, as shown by SOMs *A*–*F* in Fig. 2.

Thus, we only need to discuss the corresponding BCs of SOMs at different starting positions with undulating heights. In this way, we obtain BCs of each SOM in the middle position, such as the red rectangle in the middle of SOM *A* and the green one in the middle of SOM *B* in Fig. 2. For the rectangular units at the two ends, the corresponding BCs in the two SOMs at the two ends in Fig. 2 are directly retained. By splicing the IBCs at each step distance on the undulating terrain, the BCs of the complete terrain can be obtained.

Combining the BC equations (5) and (6) in Section III-A, the problem is unified to solve the parameters K, H , and Λ in SOMs with different starting positions and heights.

IV. Machine Learning of the BCs

Considering that the BCs of SOMs should be determined by different obstacle environments, we introduce a machine learning method to explore their relationships.

A. Derivation of BCs

The propagation paths of the waves that are incident on the boundaries of an SOM are shown in Fig. 4. It can be seen from Fig. 4 that the boundaries connected to free space (Ω_1) of SOM (Ω_2) may be affected by both upward waves in green and downward waves in purple, whereas the boundaries connected to ground are only affected by downward waves in blue.

1) Downward Waves on the Boundary: The downward wave on the boundary can be decomposed into plane waves from multiple directions. We only discuss the situation in which there are decomposed plane waves incident from two directions θ_{p1} and θ_{q1} for simplicity, as shown in the magnified SOM in Fig. 4. The corresponding refraction angles are, respectively, θ_{p2} and θ_{q2}. Thus, IBCs obtained by downward waves, respectively, in Ω_1 and Ω_2 are expressed as [7]

$$\begin{cases} \frac{\partial u_{p1}}{\partial z} + \frac{\Gamma_1}{\tilde{\varepsilon}_{r2}} \cdot u_{p1} = 0 \\ \frac{\partial u_{p1}}{\partial z} + \Gamma_1 \cdot u_{p1} = 0 \end{cases}, \Gamma_1 = -jk_2 \left(p \cdot \cos\theta_{p2} + (1-p) \cdot \cos\theta_{q2}\right) \tag{7}$$

where $\tilde{\varepsilon}_{r2} = \varepsilon_{r2} + \sigma_2/\mathrm{j}\omega\varepsilon_0$ is the complex permittivity of SOM medium, and p and $1-p$ are the ratios of the field strength generated by the two decomposed plane waves on the boundary to that generated by the original downward wave.

2) Upward Waves on the Boundary: Similarly, it can be assumed that there are two upward waves in the incident directions ${\theta_{p1}}'$ and ${\theta_{q1}}'$ on the boundary, and the corresponding refraction angles are ${\theta_{p2}}'$ and ${\theta_{q2}}'$, which account for p' and $1-p$' of the total upward waves on the boundary. Then, IBCs obtained by upward waves in Ω_1 and Ω_2 are, respectively

$$\begin{cases} \frac{\partial u_{p2}}{\partial z} + \Gamma_2 \cdot u_{p2} = 0 \\ \frac{\partial u_{p2}}{\partial z} + \frac{\Gamma_2}{1/\tilde{\varepsilon}_{r2}} \cdot u_{p2} = 0 \end{cases}, \Gamma_2 = jk_1 \left(p' \cdot \cos{\theta_{p2}}' + (1-p') \cdot \cos{\theta_{q2}}'\right). \tag{8}$$

3) BCs on Each Boundary: We suppose the field strengths of the downward waves and upward waves each account for a certain proportion m and $(1-m)$ of the total field strength, denoted as $u_1$and u_2

$$u_1 + u_2 = m \cdot u_{\mathrm{tol}} + (1-m) \cdot u_{\mathrm{tol}} = u_{\mathrm{tol}}. \tag{9}$$

Therefore, the IBC satisfying the total field strength on the lower boundary of Ω_1 can be written as

$$\frac{\partial u}{\partial z} + \mathrm{K} \cdot \ u = 0, \begin{cases} \mathrm{K} = m \cdot \frac{\Gamma_1}{\tilde{\varepsilon}_{r2}} + (1-m) \cdot \Gamma_2 \\ \Gamma_1 = -\mathrm{j}k_2 \left(p \cdot \cos\theta_{p2} + (1-p) \cdot \cos\theta_{q2}\right) \\ \Gamma_2 = \mathrm{j}k_1 \left(p' \cdot \cos{\theta_{p2}}' + (1-p') \cdot \cos{\theta_{q2}}'\right) \\ m, p, p' \in [0,1] \end{cases}. \tag{10}$$

Similarly, the IBC on the upper boundary of Ω_2 is

$$\begin{cases} \frac{\partial u}{\partial z} + \mathrm{H} \cdot \ u = 0 \\ \mathrm{H} = \mathrm{m} \cdot \Gamma_1 + (1-\mathrm{m}) \cdot \Gamma_2 \cdot \tilde{\varepsilon}_{r2} \end{cases}. \tag{11}$$

For the lower boundary of Ω_2, assuming that parameters of the ground are ε_3, μ_3 , and σ_3. The incident angles of two downward waves are ${\theta_{p1}}''$ and ${\theta_{q1}}''$, and the refraction angles are ${\theta_{p2}}''$ and ${\theta_{q2}}''$, accounting for p" and $1-p$" similarly. The IBC is

$$\begin{cases} \frac{\partial u}{\partial z} + \frac{\Lambda}{\tilde{\varepsilon}_{r3}} \cdot u = 0 \\ \Lambda = -jk_3 \left(p'' \cdot \cos{\theta_{p2}}'' + (1-p'') \cdot \cos{\theta_{q2}}''\right) \end{cases} \tag{12}$$

where $\tilde{\varepsilon}_{r3} = \varepsilon_{r3} + \sigma_3/j\omega\varepsilon_0$ is the complex permittivity of the medium ground. Thus, according to (10)–(12) solving the parameters can be converted into solving angles and proportions of waves on the boundaries of SOMs as shown in Fig. 4.

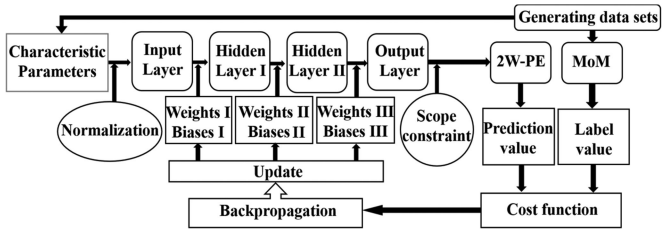

Fig. 5. Flowchart of machine learning.

TABLE I
PARAMETERS OF SOM($3\Delta_x$)

Parameters	Symbols	Ranges & Steps
Obstacle height 1	h_1	$[1:1:100]$
Obstacle height 2	h_2	$[h_1-2:1:h_1+2]$
Obstacle height 3	h_3	$[h_2-2:1:h_2+2]$
Start position of SOM	d	$[550:50:650]$

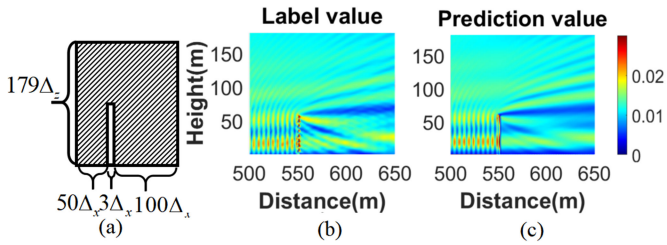

Fig. 6. Schematic diagram of calculation area and field value comparison. (a) Calculation range. (b) Label field by MoM. (c) Prediction field by 2W-PE.

B. Design of Neural Network

We design an ANN that can adaptively determine the parameters existing on the boundaries in different SOMs. Fig. 5 shows the flowchart of machine learning ANN to determine the BC and improve the prediction.

First, we set the input layer feature parameters as: the starting position of SOMs d and the corresponding heights of SOM at three steps h_1, h_2, and h_3. Since the width of the SOM is only $3\Delta_x$, $\Delta_x = \Delta_z = 1$, and the terrain will not be steep, the adjacent undulation of SOM will not exceed two grids, except at the start and end of obstacles. The transmitter height h_t, beam width θ_{bw}, elevation angle θ_{elv}, working frequency f, and terrain electrical parameters $(\varepsilon_r, \mu_r, \sigma)$are supposed to be fixed. The variable names and ranges for training are given in Table I. Assuming that the upper half of the space is free space, the ground and obstacle have the same conductivity 10^{-5} S/m, the same permeability μ_0 , but different relative permittivity values of 6 and 4; the working frequency is 30 MHz, and equivalent radiation power of the radiation source is $1/120\pi$W. We also obtain the datasets by MoM as the label value under above different parameters for training. To reduce the amount of calculation, we mainly concern the field strength by MoM in the area around the obstacle as shown in Fig. 6(a).

The final outputs are 12 proportions and 18 angle parameters of waves on the boundaries of the SOM as shown in Fig. 4. Each proportion is considered as a complex number to be output in real and imaginary parts, so there are 42 outputs in total. Meanwhile, the outputs of ANN are inputs of 2W-PE, so the predicted field

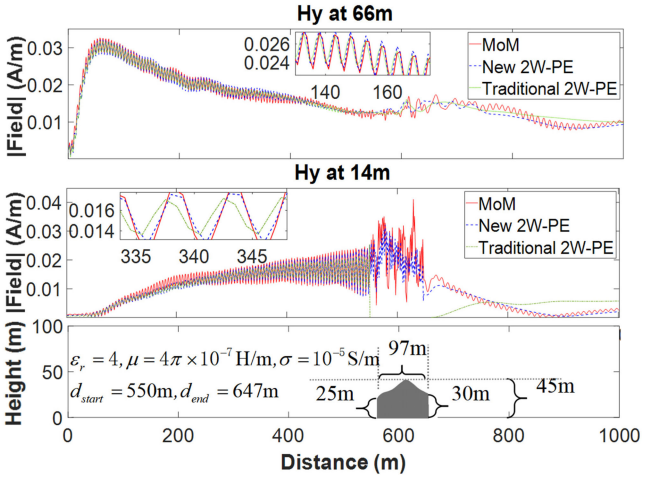

Fig. 7. Comparison of field strength in single obstacle environment.

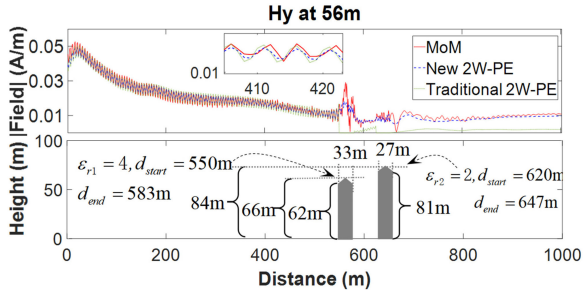

Fig. 8. Comparison of field strength in two obstacles environment.

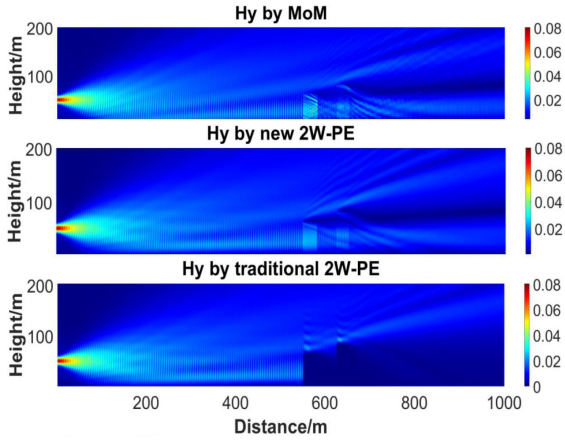

Fig. 9. Comparison of field strength distributions.

value in the selected area can be obtained by 2W-PE. As our problem is a nonlinear regression problem, the cost value can be set as the relative value of the two-norm of the label and calculation values' difference. Then, we can use DMFT and FD to solve 2W-PE with trained boundary parameters to obtain the spatial field.

V. Simulation Results

We randomly select 1200 datasets as the training set and 300 datasets as the validation set. After ten rounds of training, we calculate an average accuracy rate of 87.6% on the training set and 87.1% on the validation set. Here, we compare a sample in which the SOM is at 550 m and the heights are 60, 61, and 59 m. The label value and prediction value are shown in Fig. 6(b) and (c). The corresponding spatial field distributions and paths of reflection and refraction are almost the same, and the accuracy rate in this case is 88.6%.

Example 1: For the single obstacle environment shown in Fig. 7, we obtain the BC parameters from the trained ANN, and we compare the results of the new 2W-PE with MoM and the traditional 2W-PE at the observation heights of 14 and 66 m. From the result at 14 m, the overall consistency of the new 2W-PE with MoM is significantly better than that of the traditional 2W-PE with MoM. There is a significant error in front of and behind the obstacle in the result of the traditional 2W-PE, which is a result of ignoring the internal field value. When observing at 66 m beyond the obstacle, the traditional 2W-PE still produces some obvious errors in the upper area, whereas the new 2W-PE and MoM maintain better consistency. The average calculation time of MoM is 3002 s, and that of the new 2W-PE is 26 s, demonstrating the superior speed of the new 2W-PE. MoM of the media ground needs to use the discrete complex image method to solve the Sommerfeld integral, so the calculation is large, and it can only be applied at close range as a verification method. The new 2W-PE is mainly calculated from the Fourier transformation, so the efficiency is significantly improved.

Example 2: For the environment as shown in Fig. 8, there are two undulating obstacles with the same conductivity 10^{-5} S/m, and same permeability μ_0, which have different relative dielectric constants of 4 and 2. The specific sizes of obstacles are shown in Fig. 8. The field values calculated by the three methods at the observation height of 56 m in front of the obstacle are in good agreement, but between the two obstacles and in the space behind the obstacles, new 2W-PE is more consistent with MoM than the traditional 2W-PE.

Finally, in the obstacle environment corresponding to Fig. 8, we draw the field distributions of MoM and the two 2W-PE methods in the entire space in Fig. 9. Compared with the results of the traditional 2W-PE from [7], the new 2W-PE is more accurate in the entire space, which is the result of considering the internal propagation and choosing appropriate BCs. The calculation mesh of MoM is finer, so its accuracy display has a higher resolution.

VI. Conclusion

A new 2W-PE method based on machine learning to predict the spatial field value is introduced, which is tested against MoM and traditional 2W-PE. The new method includes longitudinal decomposition calculation and lateral expansion processing. In the former, the DD algorithm is used to solve 2W-PE at each step distance; in the latter, we introduce the SOM and achieve the approximation of various undulating terrains by using the overlay combination and lateral extension of multiple SOMs. Then, machine learning is introduced to help determine the parameters of the BCs in SOMs, which makes the prediction more accurate and able to be generalized to arbitrary terrain.

REFERENCES

[1] O. Ozgun, "Recursive two-way parabolic equation approach for modeling terrain effects in tropospheric propagation," *IEEE Trans. Antennas Propag.*, vol. 57, no. 9, pp. 2706–2713, Sep. 2009.

[2] O. Ozgun, G. Apaydin, and M. Kuzuoglu, "PETOOL: MATLAB-based one-way and two-way split-step parabolic equation tool for radiowave propagation over variable terrain," *Comput. Phys. Commun.*, vol. 182, no. 9, pp. 2638–2654, Jan. 2011.

[3] G. Apaydin and L. Sevgi, "Two-way propagation modeling in waveguides with three-dimensional finite-element and split-step Fourier-based PE approaches," *IEEE Antennas Wireless Propag. Lett.,* vol. 10, pp. 975–978, 2011.

[4] K. Wang and Y. L. Long, "Propagation modelling over irregular terrain by the improved two-way parabolic equation method," *IEEE Trans. Antennas Propag.*, vol. 60, no. 9, pp. 4467–4471, Sep. 2012.

[5] Q. F. Wei, C. Y. Yin, and W. Wu, "Research and verification for an improved two-way parabolic equation method in obstacle environment," *Microw., Antennas Propag.*, vol. 12, no. 4, pp. 576–582, 2018.

[6] A. Q. Li, C. Y. Yin, Y. J. Gan, and W. Wu, "Accurate prediction of radio wave propagation in an environment of dielectric ground and obstacles based on the principle of domain decomposition," *Microw., Antennas Propag.*, vol. 15, pp. 1473–1489, 2021, doi: 10.1049/mia2.12130.

[7] A. Q. Li, C. Y. Yin, Q. Q. Zhang, and Y. J. Gan, "Research on fast algorithm of radio wave propagation in low-lossy obstacles environment," *Int. J. Antennas Propag.*, vol. 2021, Apr. 2021, Art. no. 5519586.

[8] H. Singh, S. Gupta, C. Dhawan, and A. Mishra, "Path loss prediction in smart campus environment: Machine learning-based approaches," in *Proc. IEEE 91st Veh. Technol. Conf.*, 2020, pp. 1–5.

[9] S. P. Sotiroudis and S. K. Goudos, "Application of a composite differential evolution algorithm in optimal neural network design for propagation path-loss prediction in mobile communication systems," *IEEE Antennas Wireless Propag. Lett.*, vol. 12, pp. 364–367, 2013.

[10] M. Levy, *Parabolic Equation Methods For Electromagnetic Wave Propagation*. London, U.K.: IET Digital Library, 2000.

[11] C. Y. Yin, J. Zhu, and Q. F. Wei, "Study on calculation and verification of radiowave propagation using parabolic equation for the antenna near the ground," in *Proc. 37th Prog. Electromagn.*, Aug. 2016, pp. 655–1659.

[12] D. Dockery and J. R. Kuttler, "An improved impedance-boundary algorithm for Fourier split-step solutions of the parabolic wave equation," *IEEE Trans. Antennas Propag.*, vol. 44, no. 12, pp. 1592–1599, Dec. 1996.